JMEPEG (2009) 18:1041–1045
DOI: 10.1007/s11665-008-9348-8

1059-9495/$19.00

Synthesis and Characterization of Air-Sintered Al_2O_3-Bronze Composites

A. Shrestha, R. Asthana, T.K. Lacksonen, and M. Singh

(Submitted December 11, 2008)

Powder blends of Al_2O_3 and a Cu-Sn-Pb bronze (0-20% bronze) were cold compacted and air-sintered at 1473-1773 K. The Al_2O_3-bronze composites exhibited networks of metal microchannels, some porosity, and diffusion of Pb in Al_2O_3 and of Al and O in bronze. The hardness of un-doped Al_2O_3 increased linearly with temperature, from 455 Knoop microhardness (HK) at 1473 K to 2010 HK at 1773 K, but the hardness of the Al_2O_3/bronze composite exhibited a sluggish, nonlinear dependence on temperature, with a peak hardness of 1150 HK at 1673 K. Air sintering may be viable to synthesize Al_2O_3/bronze composites with low bronze contents

Keywords composites, energy dispersive spectroscopy, microhardness, pressing, scanning electron microscopy, sintering

Dispersions of metallic second phase particles in ceramics improve the latter's toughness via crack deflection and crack bridging. There has been interest in Al_2O_3-matrix composites containing Cu dispersions because of toughness enhancement even at small Cu contents (Ref 1-8). Cold compaction and sintering (Ref 1, 2), hot pressing (Ref 3-6), and melt infiltration (Ref 7) have been used to synthesize the Al_2O_3/Cu composites to provide toughness, strength, hardness, and thermal shock resistance.

Studies on dispersions of Cu alloys in Al_2O_3 are, however, scarce. Dispersions of alloys such as CuPbSn bronze in Al_2O_3 could reduce the friction and wear in moving ceramic parts without significant weight penalty or loss of mechanical properties relative to pure Cu dispersions. Tin in Cu forms a solid solution and improves the hardness, strength, and ductility via α (soft) and δ (hard) phases. Lead is self-lubricating, dissolves sparingly in Cu-Sn alloys, and is nearly completely rejected by Cu during solidification which permits it to be localized between grains for anti-friction applications.

The purpose of this study was to synthesize Al_2O_3-bronze composites via powder compaction and air sintering. Air sintering was implemented to permit reactive formation of thermodynamically stable oxides of Cu and alloying elements of bronze for enhanced oxidation resistance. Air sintering was considered viable because Cu-O alloys are known to wet and adhere to Al_2O_3, thus permitting densification via capillary flow in intergranular regions of the Al_2O_3.

A. Shrestha, DC Group Inc., Orlando, FL 32826; **R. Asthana**, Department of Engineering and Technology, 326 Fryklund Hall, University of Wisconsin-Stout, Menomonie, WI 54751; **T.K. Lacksonen**, Department of Operations, Construction and Management, University of Wisconsin-Stout, Menomonie, WI 54751; and **M. Singh**, Ohio Aerospace Institute, Cleveland, OH 44135. Contact e-mail: asthanar@uwstout.edu.

High-leaded tin bronze atomized powder (Aldrich Co.) of nominal size ~10 μm, and coarse nanometeric MgO-doped Al_2O_3 (Reynold's Metals Co., Bauxite, AZ) of nominal size 380 nm were used as the raw materials. The powders were mixed in various proportions using mortar and pestle and compacted under a pressure of 175 MPa into 29 mm diameter × 6-7 mm thick discs using a hydraulic press and tool steel dies. Air sintering was done in a programmable furnace at 1573-1773 K (composite) and 1473-1773 K (monolithic Al_2O_3) for soak periods of 0.5-4 h. Sintered coupons were characterized for bulk density using the Archimedes method, and microstructure and composition using scanning electron microscopy (JEOL JSM 840A) coupled with energy dispersive spectroscopy (EDS). Polished specimens were tested for microhardness on a Buehler MicroMet-2001 machine using a Knoop microindentor (200 g load, 10 s), and the average of 8-10 measurements on each sample was taken to represent the hardness.

The SEM images of as-received bronze and alumina (Fig. 1) show some agglomeration. The nominal compositions (in at.%) of alumina and bronze from EDS are 67.39% Al-32.11O-0.496Mg and 78.98Cu-12.28Sn-8.44Pb-0.31Zn, respectively (in wt.%, the bronze composition is 60.94Cu-21.1Pb-17.7Sn-0.24Zn, which is similar to that of alloy C94500 (Ref 9) but with excess tin, which strengthens Cu).

The density (Fig. 2) of the composites is lower than the density of pure Al_2O_3 because of residual porosity and visually observable cracking especially at high (>10%) bronze contents similar to the literature studies (Ref 1-3) on Al_2O_3/pure Cu composites. The density of 0% and 5% bronze composites slightly increased with increasing temperature, with the density of the 5% composite increasing at a slower rate than that of pure Al_2O_3. The density of the 20% bronze composites (exhibiting the most cracking) was lower than the density of the 10% bronze composites. The origin of the cracks can be traced to several factors. The differential expansion between bronze (CTE ~18.5 ppm/K) and Al_2O_3 (CTE ~8.1 ppm/K) upon heating to the alloy solidus (T_S ~1073 K) shall create internal stresses prior to neck formation between Al_2O_3 powders that are held together via a purely

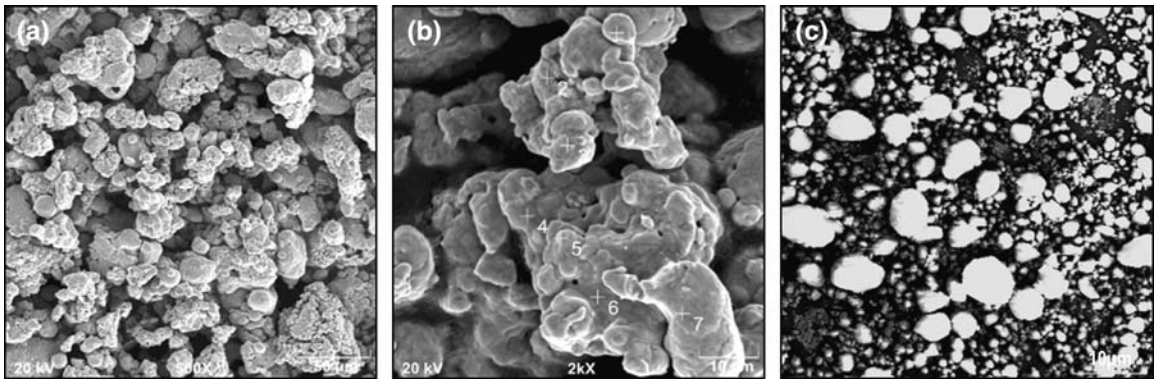

Fig. 1 (a and b) High-leaded bronze powder, and (c) high-purity Al_2O_3 powder. The average powder compositions based on the EDS analysis are (in at.%): 78.98Cu-12.28Sn-8.44Pb-0.31Zn for bronze and 67.39Al-32.11O-0.49 Mg for alumina

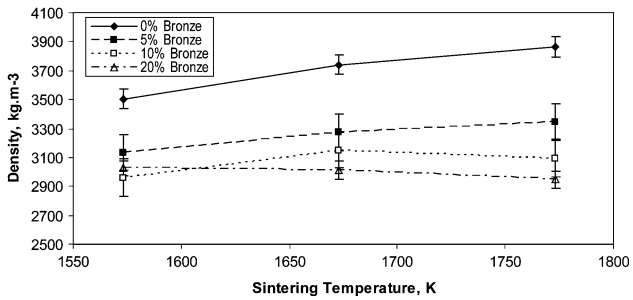

Fig. 2 Density of sintered Al_2O_3/bronze composites as a function of sintering temperature

frictional bond. Additionally, extensive volatilization of lead, copper, tin, and zinc above 1473 K (Ref 10) could create internal gas pressure and pore and crack formation. Residual stresses from CTE mismatch during post-sinter cooling could also induce cracks.

The phase distribution in the composites is inhomogeneous (Fig. 3a) with bright metal-rich zones separated by metal-impoverished regions and dispersed porosity. The inhomogeneity results from uneven powder mixing prior to cold compaction. In pore-free areas, the metal has invaded the intergranular regions, thus creating an interpenetrating network of metal microchannels within the Al_2O_3 matrix. The metal interlayers appear to be well bonded to Al_2O_3 grains. At the highest sintering temperature of 1773 K, liquid bronze between Al_2O_3 grains shall superheat by almost 773 K and disintegrate into island-like films because of reduced surface tension and increased fluidity, leading to finely dispersed shrinkage porosity at the Al_2O_3 grain junctions.

The dark regions in the photomicrographs of Fig. 3 are Al_2O_3-rich areas that also contain some lead (5-7%) and, in a few cases, tin (Fig. 3f). The light regions are mostly a Cu-rich phase that contains Pb, Al and O, with Al and O enrichments possibly resulting from the dissolution of Al_2O_3 in molten bronze. The light regions in Fig. 3(c) and (f) are actually Sn-rich areas and contain O, Al and Pb, and in some cases, a small amount of Cu. The presence of Pb in the Al_2O_3 grains and of Al and O in bronze films between the Al_2O_3 grains suggests that interdiffusion and redistribution of chemical species has taken place during sintering.

The diffusional rearrangement will affect the spreading and capillary flow in the intergranular regions of the Al_2O_3. Pure Cu does not wet Al_2O_3 (contact angle, $\theta \sim 128°$ at 1423 K, Ref 11). The dissolution of Al in Cu decreases the θ, which drops to 80° at 1423 K at $X_{Al} = 0.4$ (X: mole fraction) (Ref 12) thus making the system wettable. Similarly, O dissolution in molten Cu lowers the θ (Ref 13-22) by forming wettable interfacial oxides and aluminates and the θ decreases with increasing p_{O_2}. At high ($\sim$10.5 wt.%) O contents, θ in the Al_2O_3/Cu-O system drops to 12° and a high work of adhesion (1340 mJ m^{-2}) is attained. In the case of Sn on Al_2O_3, at low T ($<$1000 K), θ is large ($\sim$140°) because of a tenacious SnO_2 film on Sn which restricts spreading (Ref 12). Above 1073 K, however, the oxide dissolves in molten Sn, thus increasing the O concentration in Sn and decreasing the θ ($\sim$110°) (Ref 12). Because both Cu and Sn are nonwetting and nonreactive to Al_2O_3, Cu-Sn alloys also do not wet the Al_2O_3; even at 1423 K, Sn in Cu only marginally decreases the θ from 129° at 0% Sn to 122° at $X_{Sn} = 0.4$ (Ref 23). In a manner similar to Cu and Sn, Pb also does not wet Al_2O_3 ($\theta \sim 117$-132°, Ref 24).

What emerges from this discussion is that there are two opposing factors that influence the wettability and densification of Al_2O_3 in the presence of liquid bronze: Sn and Pb impair the wettability and capillary flow but O and Al in Cu facilitate the wettability with Al_2O_3.

Air sintering of Al_2O_3/bronze composites could form oxides such as Cu_2O, CuO, Cu_3O_2, SnO_2, SnO, PbO, Pb_3O_4, and PbO_2. The Gibb's free energy (ΔG) of formation (per mole of the element) calculated as a function of temperature using the software HSC Chemistry version 4.1 (Outokumpu Research Oy, Pori, Finland) showed that SnO_2 is the most stable oxide up to 1773 K, followed by SnO, PbO, and Pb_3O_4 in that order. PbO_2 becomes unstable ($\Delta G > 0$) above 1473 K, and CuO becomes unstable near 1773 K. A number of these oxides have low melting points, and they will likely promote liquid phase sintering, thus enhancing the sintering kinetics and grain coarsening. Oxides such as Pb_3O_4 (M.P.: 773 K), PbO (M.P.: 1159 K), SnO (M.P.: 1353 K), SnO_2 (M.P.: 1400 K), CuO (M.P.: 1474 K), and Cu_2O (M.P.: 1508 K) will melt during sintering. Oxides such as PbO (boiling points: 1743 K) could evaporate causing internal gas pressure, void formation, and distortion and cracking.

Besides simple binary oxides, copper aluminates, $CuAl_2O_4$ spinel and $CuAlO_2$, may also form (Ref 15, 16, 18) (ΔG for these could not be calculated because the software lacked the

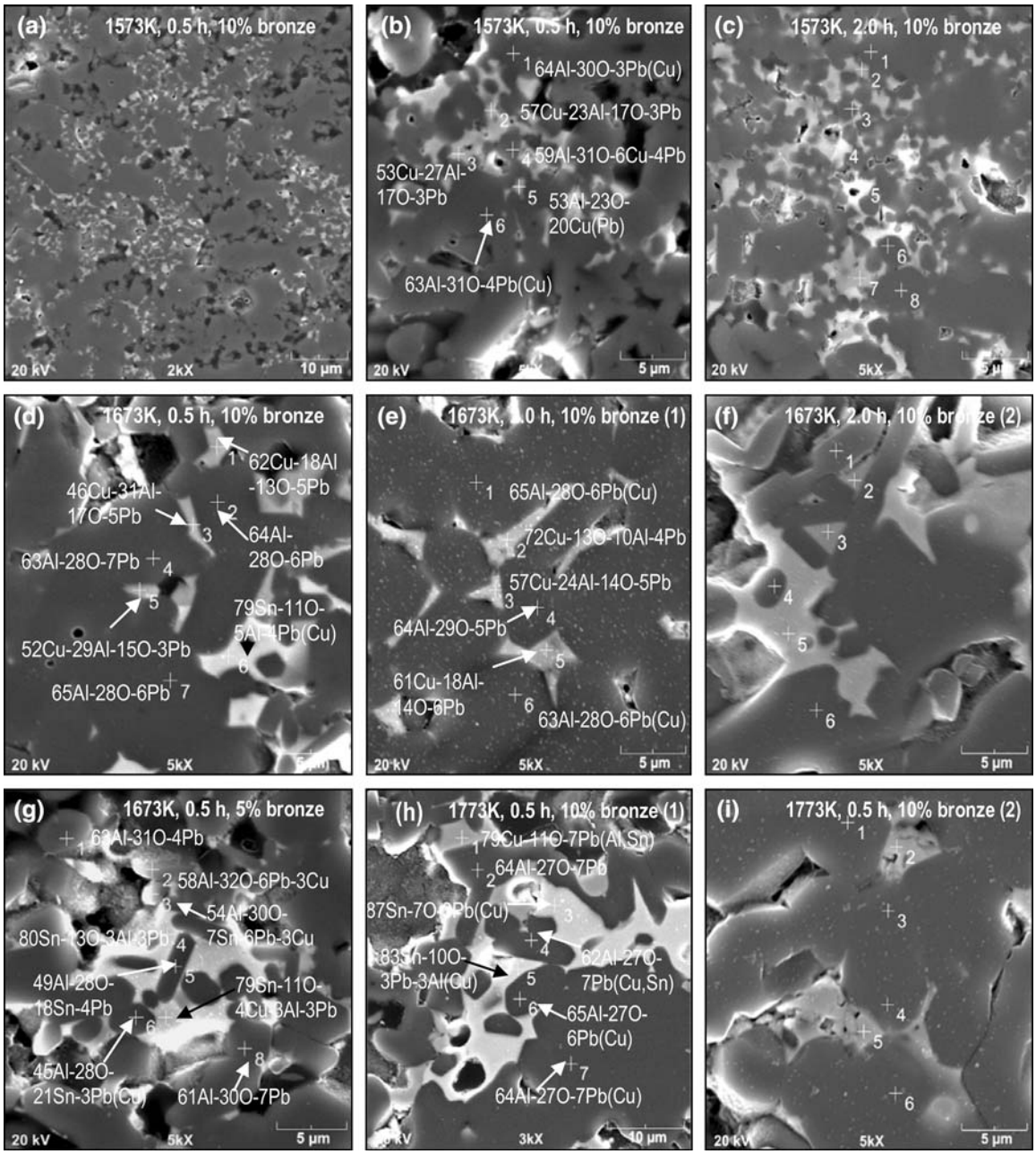

Fig. 3 SEM images of the Al_2O_3/bronze composites sintered under different conditions. Elemental compositions (in at.%) from EDS analyses at point markers are shown for some samples; minor elements (<2 at.%) are shown in parentheses. For a few samples, two representative regions marked (1) and (2) are shown

needed thermo-physical data). These aluminates together with oxides can cause residual stresses due to the volumetric changes in phase transformation and the CTE mismatch between the Al_2O_3 and the reaction products. Even in pure Cu/Al_2O_3 samples, Al_2O_3 is subjected to stress by CuO, Cu_2O, and $CuAlO_2$ at the interface (Ref 18). The magnitude of the stress caused by $CuAlO_2$ and CuO is less than that caused by Cu_2O. The CTE values (Ref 18) along the *a* and *c* axes of α-Al_2O_3 (hexagonal) are 8×10^{-6}/K and 9×10^{-6}/K, respectively, and the CTE of cubic Cu and cubic Cu_2O are 23×10^{-6}/K and 3×10^{-6}/K, respectively. In addition, the CTE of CuO (monoclinic) is 12×10^{-6}/K (*a*-axis), 7×10^{-6}/K (*b*-axis), and 7×10^{-6}/K (*c*-axis), and the CTE of $CuAlO_2$ (hex) is 12×10^{-6}/K (*a*-axis) and 6×10^{-6}/K (*c*-axis). The thermal strains $\Delta\alpha\Delta T$ ($\Delta\alpha$: CTE mismatch, ΔT: temperature excursion) could thus be large and anisotropic, and give rise to residual stresses.

Figure 4(a) shows the Knoop microhardness (HK) of monolithic Al_2O_3 and Al_2O_3/10% bronze composites as a function of sintering temperature. The increase in HK with temperature over 1473-1773 K for pure Al_2O_3 is roughly linear, and follows the equation: $HK = 5.1836T - 7110$ ($R^2 = 0.9324$). For the composite, hardness only marginally depends on temperature, reaches a maximum (1150 HK) at 1673 K, and slightly declines at 1773 K. The decrease in the composite's hardness at 1773 K is due to Al_2O_3 grain

coarsening and associated pore formation which are accelerated in the presence of liquid films that facilitate diffusion. A marked difference in the Al_2O_3 grain size is revealed in the fracture surfaces (Fig. 5a and d) of the composite and monolithic Al_2O_3; grains are uniform and significantly finer in monolithic Al_2O_3. Grain coarsening and pore formation occur at higher temperatures in pure Al_2O_3; as a result, hardness does not peak even at 1773 K. Fracture appears to be predominantly intergranular in both Al_2O_3 and the composite (Fig. 5) with sharp faceted grain edges and grain corners visible.

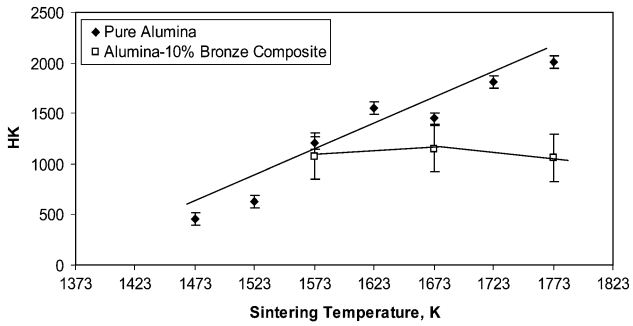

Fig. 4 Knoop microhardness vs. sintering temperature in Al_2O_3 and Al_2O_3/bronze composite

In summary, Al_2O_3-matrix composites containing 0-20% bronze (Cu-Sn-Pb) dispersions, synthesized via cold compaction and air sintering (1473-1773 K, 0.5-4.0 h) exhibited metal penetration of Al_2O_3 grain boundaries and diffusion of Pb in Al_2O_3 and of Al and O in bronze, but also porosity and cracking, especially at high bronze contents which led to a decrease in the material's density. Whereas pure Al_2O_3 attained high hardness (2010 HK at 1773 K), the Al_2O_3/bronze composites exhibited relatively low hardness (823-1458 HK) and a sluggish dependence on sintering temperature and bronze content. Air sintering may be viable to synthesize Al_2O_3/bronze composites at low (≤10%) bronze contents.

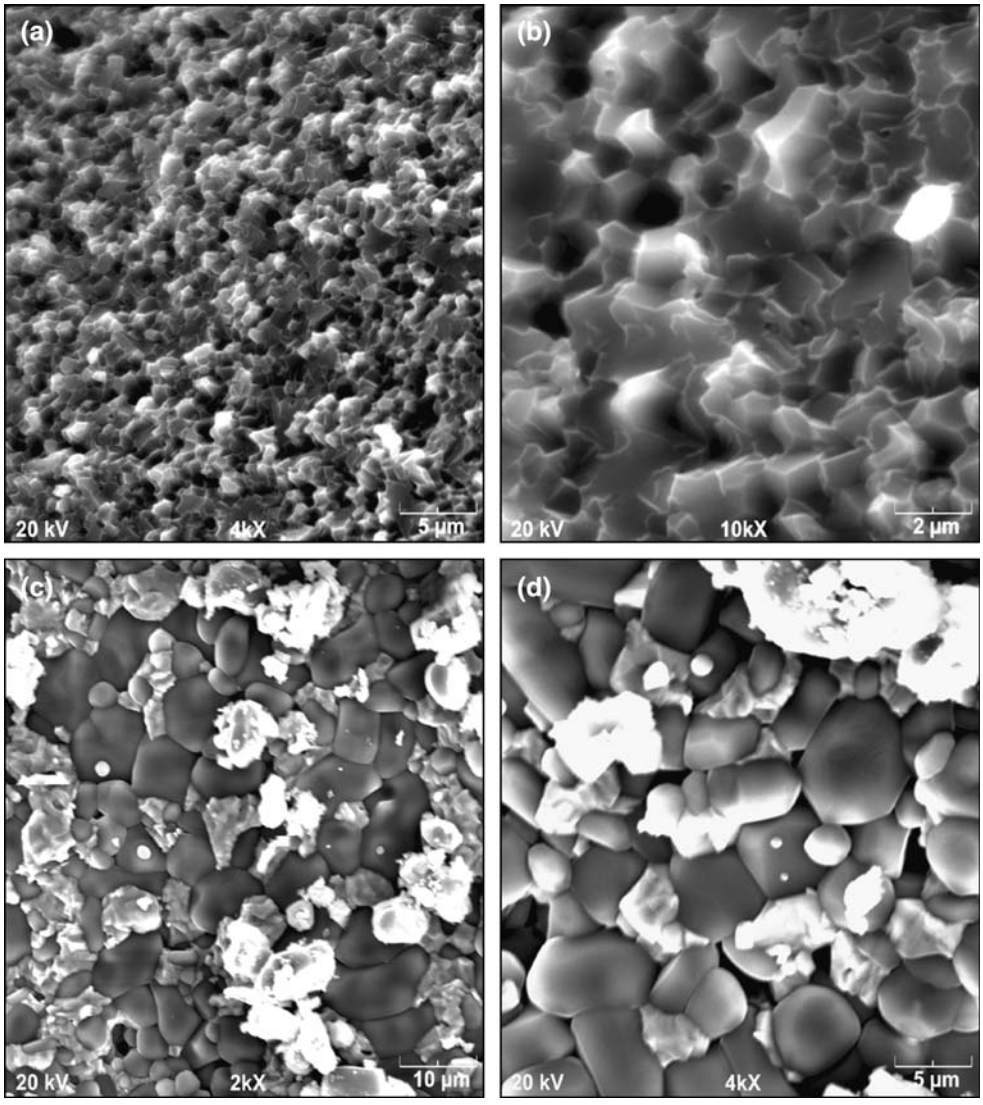

Fig. 5 Fracture surfaces of (a and b) pure Al_2O_3 and (c and d) Al_2O_3/10% bronze composite sintered at 1673 K for 0.5 h

Acknowledgment

The authors would like to thank Reynold's Metals Co., Bauxite, AZ, for the gift of the alumina powders.

References

1. J.G. Miranda-Hernandez, S. Moreno-Guerrero, A.B. Soto Guzman, and E. Rocha Rangel, Production and characterization of the Al_2O_3-Cu composite material, *J. Ceram. Proc. Res.*, 2006, **7**(4), p 311–314
2. S. Moreno-Guerrero, L.N. Couvert, J.G. Miranda-Hernandez, and E. Rocha Rangel, Production and Characterization of Al_2O_3-Based Composites Reinforced with Different Metals, N.P. Bansal et al. Eds., *Materials and Systems: Proceedings of the International Symposium on CMC's*, MS&T 2007, American Society for Materials, Materials Park, OH, 2007, p 327-337
3. H. Lu, H. Sun, C. Chen, R. Zhang, D. Yang, and X. Hu, Coating Cu Nano-Sized Particles on Al_2O_3 Powders by a Wet-Chemical Method and Its Mechanical Properties After Hot Press Sintering, *Mater. Sci. Eng. A*, 2006, **426**(1–2), p 181–186
4. L. Wang, J.L. Shi, M.T. Lin, H.R. Chen, and D.S. Yan, The Thermal Shock Behavior of Alumina-Copper Composite, *Mater. Res. Bull.*, 2001, **36**(5–6), p 925–932
5. J.F. Silvain, J.L. Bobet, and J.M. Heintz, Electroless Deposition of Copper onto Alumina Sub-Micronic Powders and Sintering, *Compos. A: Appl. Sci. Manuf.*, 2002, **33**(10), p 1387–1390
6. D.Y. Ying and D.L. Zhang, Processing of Cu-Al_2O_3 Metal Matrix Nanocomposite Materials by Using High Energy Ball Milling, *Mater. Sci. Eng.*, 2000, **A286**, p 152–156
7. N.A. Travitzky, Microstructure and Mechanical Properties of Alumina/Copper Composites Fabricated by Different Infiltration Techniques, *Mater. Lett.*, 1998, **36**(1–4), p 114–117
8. M.A. Ritland and D.W. Readey, Alumina-Copper Composites by Vapor Phase Sintering, *Ceram. Eng. Sci. Proc.*, 1993, **4**(9–10), p 896–907
9. A. Cohen, "Properties and Selection: Nonferrous Alloys and Special-Purpose Materials," Vol. 2, *ASM Handbook*, 1988, ASM International, Materials Park, OH, USA, p 382
10. O. Barin, H. Wilhelmi, and I. Barin, Mass Transfer From Copper Melts by Top-Blowing of an Argon-Hydrogen Plasma Jet, *Plasma Chem. Plasma Process.*, 1991, **11**(4), p 545–559
11. N. Eusthapoulos, M. Nicholas, and B. Drevet, *Wettability at High Temperatures*, Pergamon Materials Series, Vol. 3, Pergamon, Oxford, UK, 1991
12. I. Rivollet, D. Chatain, and N. Eustathopoulos, Wettability of Alumina Single Crystals with Gold and Tin, *Acta Mater.*, 1987, **35**, p 835
13. M. Diemer, A. Neubrand, K. Trumble, and J. Roedel, Influence of the Oxygen Content on the Wettability in the Copper-Oxygen-Alumina System, *J. Am. Ceram. Soc.*, 1999, **82**, p 2825–2832
14. V. Ghetta, J. Fouletier, and D. Chatain, Oxygen Adsorption Isotherms at the Surfaces of Liquid Cu and Au-Cu Alloys and Their Interfaces with Al_2O_3 Detected by Wetting Experiments, *Acta Mater.*, 1996, **44**(5), p 1927–1936
15. M.D. Baldwin, P.R. Chidambaram, and G.R. Edwards, Spreading and Interlayer Formation at the Copper-Copper Oxide/Polycrystalline Alumina Interface, *Metall. Mater. Trans. A*, 1994, **25**(11), p 2497
16. K.A. Rogers, K.P. Trumble, B.J. Dalgleish, and I.E. Reimanis, Role of Oxygen in Microstructure Development at Solid-State Diffusion-Bonded Cu/α-Al_2O_3 Interfaces, *J. Amer. Ceram. Soc.*, 1994, **77**(8), p 2036–2042
17. P. Chidambaram, A. Meir, and G.R. Edwards, The Nature of Interfacial Phenomena at Cu-Ti/Alumina and Cu-O/Alumina Interfaces, *Mater. Sci. Eng. A*, 1996, **206**, p 249–258
18. T. Fujimura and S.I. Tanaka, In-Situ High-Temperature X-Ray Diffraction Studies Cu/Al_2O_3 Interface Reactions, *Phil. Mag. A*, 1991, **64**(3), p 561–576
19. P.D. Ownby, and J.J. Liu, Surface Energy of Liquid Copper and Single Crystal Sapphire and the Wetting Behavior of Copper on Sapphire, *Adhesion Sci. Technol.*, 1998, **2**, p 255
20. C.M. Beraud, M. Courbier, C. Esnouf, D. Juve, and D. Treheux, Study of Copper-Alumina Bonding, *J. Mater. Sci.*, 1989, **24**(12), p 4545–4554
21. S.P. Mehrotra and A.C.D. Chaklader, Interfacial Phenomena Between Molten Metals and Sapphire Substrate, *Metall. Trans.*, 1987, **B16**, p 567
22. A.C.D. Chakladar, A.M. Armstrong, and S.K. Misra, Interface Reactions Between Metals and Ceramics: IV. Wetting of Sapphire by Liquid Copper-Oxygen Alloys, *J. Amer. Ceram. Soc.*, 1968, **51**(11), p 630–634
23. J.G. Li, L. Coudurier, and N. Eustathopoulos, Work of Adhesion and Contact Angle Isotherm of Binary Alloys on Ionocovalent Oxides, *J. Mater. Sci.*, 1989, **24**, 1109
24. D. Chatain, I. Rivollet, and N. Eustathopoulos, *J. Chim. Phy.*, 1986, **83**, p 561